

# **UC Berkeley**

## **UC Berkeley Previously Published Works**

### **Title**

Effects of catalyst crystal structure on the oxidation of propene to acrolein

### **Permalink**

<https://escholarship.org/uc/item/15z4k8q1>

### **Authors**

Zhai, Zheng  
Wütschert, Maïté  
Licht, Rachel B  
et al.

### **Publication Date**

2016-03-01

### **DOI**

10.1016/j.cattod.2015.06.011

Peer reviewed



## Effects of catalyst crystal structure on the oxidation of propene to acrolein



Zheng Zhai, Maïté Wütschert, Rachel B. Licht, Alexis T. Bell\*

Department of Chemical and Biomolecular Engineering, The University of California Berkeley, Berkeley, CA 94720-1462, USA

### ARTICLE INFO

**Article history:**

Received 16 March 2015

Received in revised form 8 June 2015

Accepted 9 June 2015

Available online 14 July 2015

**Keywords:**

Aurivillius

Selective oxidation

Bismuth molybdate

### ABSTRACT

Bismuth molybdate is known to be active for the oxidation of propene to acrolein and its activity can be altered by substitution of other elements (e.g. Fe, V, W) into the scheelite phase of  $\alpha$ -Bi<sub>2</sub>Mo<sub>3</sub>O<sub>12</sub>. This work has further revealed that the apparent activation energy for acrolein formation correlates with the band gap of the catalyst measured at reaction temperature. It is, therefore, of interest to establish how the crystal structure of the catalyst affects the activation energy. We report here an investigation of propene oxidation conducted over Bi, Mo, V oxides having the aurivillius structure with the composition Bi<sub>4</sub>V<sub>2-x</sub>Mo<sub>x</sub>O<sub>11+x/2</sub> ( $x = 0–1$ ) and compare them with oxides having the scheelite structure with the composition Bi<sub>2-x/3</sub>Mo<sub>x</sub>V<sub>1-x</sub>O<sub>12</sub> ( $x = 0–1$ ). The aurivillius-phase catalysts again show a correlation between the apparent activation energy and the band gap of the oxide, and the only difference being that for a given band gap, the apparent activation energy for the aurivillius-phase catalysts is 1.5 kcal/mol higher than that for the scheelite-phase catalysts. This difference is attributed to the lower heat of propene adsorption on the aurivillius-phase catalysts. A further finding is that for catalysts with band gaps greater than ~2.1 eV, the acrolein selectivity is ~75% for the conditions used and independent of the propene conversion. When the band gap falls below ~2.1 eV, the intrinsic selectivity to acrolein decreases rapidly and then decreases further with increasing propene conversion. This pattern shows that when the activity of oxygen atoms at the catalyst surface becomes very high, two processes become more rapid – the oxidation of the intermediate from which acrolein is formed and the sequential combustion of acrolein to CO<sub>2</sub>.

© 2015 Elsevier B.V. All rights reserved.

### 1. Introduction

The oxidation of propene to acrolein has been widely studied because of the importance of acrolein as a monomer for acrylic polymers [1,2]. The principle catalysts used to promote this reaction are bismuth molybdates in which a part of the molybdenum is substituted by one or more other metals in order to enhance the catalyst activity and selectivity [3–10]. A number of groups have investigated the mechanism of propene oxidation on  $\alpha$ -Bi<sub>2</sub>Mo<sub>3</sub>O<sub>12</sub> with the aim of understanding the elementary processes leading to acrolein and the influence of added elements on these processes [11–16]. These efforts have led to the following findings. On a fully oxidized catalyst, propene oxidation occurs via a Mars van Krevelen mechanism in which propene adsorbs reversibly and then reacts with an oxygen atom of the catalyst. This rate-limiting step leads to cleavage of one of the C–H bonds of the methyl group of

the adsorbed propene and results in the formation of an adsorbed OH group and a loosely adsorbed allyl radical that is rapidly stabilized as an adsorbed vinylalkoxide. Loss of an H atom from the latter species leads to the formation of acrolein. Consistent with this mechanism and with the observed kinetics, the rate of acrolein formation is first order in the partial pressure of propene and zero order in the partial pressure of oxygen.

Several investigations have shown that the apparent activation energy for propene oxidation to acrolein can be reduced by the replacement of Mo by Fe or V for catalysts maintaining a scheelite structure over fully oxidized catalyst [3,17–20]. We have reported in previous sections that the activation barrier for the rate-limiting step is well described by the band-gap of such catalysts, the activation energy decreasing with the band gap [21]. What is not known, though, is how the correlation might be affected by the crystal structure of the catalyst. Therefore, the present study was undertaken in order to extend the exploration of the relationship between catalyst composition/structure and catalyst activity/selectivity to a different crystal structure.

The oxide phase chosen for study is the aurivillius structure [22]. This phase has the general stoichiometry of Bi<sub>2</sub>A<sub>n-1</sub>B<sub>n</sub>O<sub>3n+3</sub>

\* Corresponding author.

E-mail address: [bell@cchem.berkeley.edu](mailto:bell@cchem.berkeley.edu) (A.T. Bell).

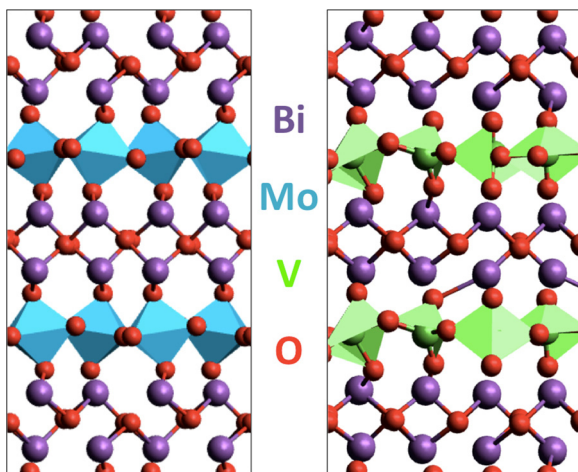


**Fig. 1.** Aurivillius crystal structures of  $\text{Bi}_2\text{MoO}_6$  (left) and distorted oxygen deficient  $\text{Bi}_4\text{V}_2\text{O}_{11}$  (right). Crystallographic data from [23] and [24].

and consists of  $n$  perovskite-like layers ( $\text{A}_{n-1}\text{B}_n\text{O}_{3n+1}$ ) sandwiched between bismuth–oxygen sheets ( $\text{Bi}_2\text{O}_2$ )<sup>2+</sup> [22]. The simplest crystal structure has  $n=1$  and corresponds to  $\text{Bi}_2\text{MoO}_6$  (the gamma phase of the bismuth molybdate) or  $\text{Bi}_2\text{WO}_6$ .  $\text{Bi}_4\text{V}_2\text{O}_{11}$  is related to the first member of the family of aurivillius compounds, but is oxygen-deficient and can be expressed as  $(\text{Bi}_2\text{O}_2)(\text{VO}_{3.5}\square_{0.5})$  [23]. Fig. 1 shows the structures of  $\text{Bi}_2\text{MoO}_6$  and  $\text{Bi}_4\text{V}_2\text{O}_{11}$  plotted using the crystal structure refinement data in references [23] and [24] respectively.  $\text{Bi}_2\text{MoO}_6$  is characterized by fluorite-like layers of  $(\text{Bi}_2\text{O}_2)^{2+}$  alternating with perovskite-like layers of  $(\text{MoO}_4)^{2-}$ . The structural similarity between  $\text{Bi}_2\text{MoO}_6$  and the distorted oxygen-deficient  $\text{Bi}_4\text{V}_2\text{O}_{11}$  is apparent from Fig. 1, where the later structure consists of  $(\text{Bi}_4\text{O}_4)^{4+}$  layers that alternate between layers of joined 4- and 5-coordinate vanadia species with overall  $(\text{V}_2\text{O}_7)^{4-}$  composition. The work presented here reveals the similarities and differences between the mechanism and kinetics of propene oxidation to acrolein over oxides having an aurivillius structure with the stoichiometry  $\text{Bi}_4\text{V}_{2-x}\text{Mo}_x\text{O}_{11+x/2}$  ( $x=0-1$ ) and oxides having a scheelite structure with the stoichiometry  $\text{Bi}_{2-x/3}\text{Mo}_x\text{V}_{1-x}\text{O}_4$  ( $x=0-1$ ).

## 2. Methods

### 2.1. Catalyst preparation

Molybdenum-substituted bismuth vanadate catalysts ( $\text{Bi}_4\text{V}_{2-x}\text{Mo}_x\text{O}_{11+x/2}$ ) were prepared by the complexation method, as described in more detail elsewhere [17]. Bismuth (III) nitrate pentahydrate ( $\text{Bi}(\text{NO}_3)_3 \cdot 5\text{H}_2\text{O}$ ) (99.98% Sigma-Aldrich), ammonium metavanadate ( $\text{NH}_4\text{VO}_3$ ) (99% Sigma-Aldrich) and ammonium molybdate tetrahydrate ( $(\text{NH}_4)_6\text{Mo}_7\text{O}_{24} \cdot 5\text{H}_2\text{O}$ ) (99.98% Sigma-Aldrich) are used as precursors. These metal precursors were mixed to achieve atomic ratios of  $\text{Bi}:V:\text{Mo}=4:(2-x):x$  in order to produce materials with the stoichiometry  $\text{Bi}_4\text{V}_{2-x}\text{Mo}_x\text{O}_{11+x/2}$ . The metal precursors were added 50 mL of water together with citric acid (1:1 molar ratio with metal precursors). The resulting solution was heated at 353 K for about 24 h in air to form a gel. The gel was then dried at 393 K and calcined in flowing air at 1023 K for 12 h. The material was then slowly cooled in air at 30 K/h to 573 K and then at 60 K/h to room temperature.

### 2.2. Catalyst characterization

X-ray diffraction patterns were obtained with a Bruker-AXS D8 Discover GADDS diffractometer using Cu K $\alpha$  radiation. Data were collected in the range of  $10^\circ < 2\theta < 80^\circ$  every  $0.02^\circ$ .

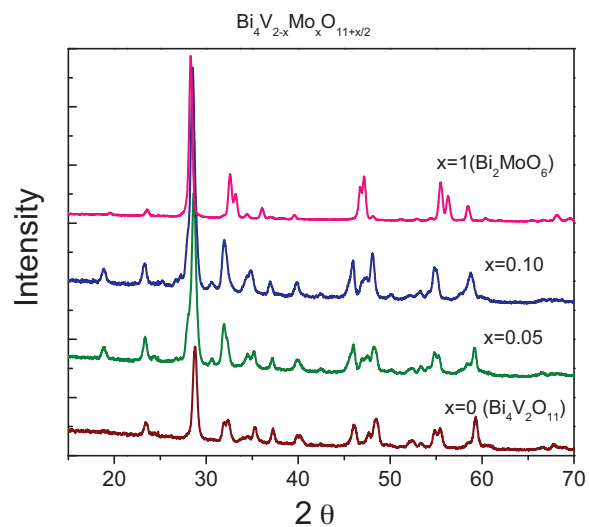


**Fig. 2.** XRD patterns of  $\text{Bi}_4\text{V}_{2-x}\text{Mo}_x\text{O}_{11+x/2}$  catalysts.

Diffuse reflectance UV–vis–NIR spectra were acquired using a Fischer Scientific EVO 300 spectrometer equipped with a Praying Mantis reflectance chamber and an in situ high-pressure cell (Harrick Scientific, Inc), fitted with quartz windows. Spectra were referenced to the diffuse reflectance spectrum of a Teflon reference tile. The procedure used to extract band-gap energies from absorption edge data is given in the Supporting Information.

### 2.3. Catalyst activity and selectivity

Measurements of reaction rates and product distributions were performed using a packed bed quartz tube reactor (10 mm in diameter) loaded with 100–800 mg of catalyst. The catalyst was preheated to the reaction temperature in air over night prior to starting a reaction. The operating temperature is between 623 and 713 K and assures that no bulk phase changes occurred in the catalyst. All experiments were carried out at atmospheric pressure with 3.3–16.7% propene (99.9%, Praxair) and 3.3–16.7% oxygen (supplied from 20% oxygen in helium, Praxair), balanced as needed with additional helium (99.995%, Praxair). Organic products were analyzed using a gas chromatograph (GC) equipped with a 30 m HP-PLOT Q column and a flame ionization detector (FID). An Alltech Hayesep DB packed column and a thermal conductivity detector (TCD) were used to analyze for oxygen, CO and CO<sub>2</sub>. Data were collected at steady-state. Conversion was calculated on the basis of products formed and product selectivity was defined as the moles of propene converted to the product over the sum of the moles of olefins converted to all products, based on a carbon balance. All selectivities reported in this study are intrinsic selectivity, extrapolated when the conversion is very low (< 1%).

## 3. Results

### 3.1. Catalyst characterization

Powder X-ray diffraction patterns of  $\text{Bi}_4\text{V}_{2-x}\text{Mo}_x\text{O}_{11+x/2}$  for  $x=0$ , 0.05, 0.1, and 1.0 are shown in Fig. 2. Comparison of these patterns with those in the literature shows that each material is a pure phase [25,26].  $\text{Bi}_4\text{V}_2\text{O}_{11}$  is stable in the  $\alpha$ -phase polymorph for temperatures of below 723 K, and therefore the diffraction pattern for this material is assigned to  $\alpha\text{-Bi}_4\text{V}_2\text{O}_{11}$ . For  $\text{Bi}_4\text{V}_{2-x}\text{Mo}_x\text{O}_{11+x/2}$ , where  $x=0.5$  and 0.1, the material is taken to be in the  $\beta$ -phase based on previous studies showing this phase to be stable for  $0.05 < x < 0.225$  [24,27].

**Table 1**

Kinetics and physical properties of  $\text{Bi}_4\text{V}_{2-x}\text{Mo}_x\text{O}_{11+x/2}$ . Note: Band-gap energies (eV) were measured at 673 K. Reaction orders in propene and oxygen were measured at 673 K for propene oxidation to acrolein. The partial pressures of propene or oxygen were fixed at 0.067 or 0.167 atm, respectively, while the other one was varied. Apparent activation energies  $E_{\text{app}}$  for propene oxidation to acrolein were measured in the temperature ranges of 623–713 K.  $P_{\text{C}_3\text{H}_6} = P_{\text{O}_2} = 0.167$  atm.

Catalyst	Band-gap $E_{\text{G}}$ (673 K)	Reaction order		$E_{\text{app}}$ (kcal/mol)
		Propene (m)	Oxygen (n)	
$\text{Bi}_4\text{V}_2\text{O}_{11}$	1.89	1.0 ± 0.1	0.1 ± 0.1	14.4
$\text{Bi}_4\text{V}_{1.9}\text{Mo}_{0.1}\text{O}_{11.05}$	1.96	1.0 ± 0.0	0.0 ± 0.0	14.9
$\text{Bi}_2\text{MoO}_6$	2.41	1.0 ± 0.0	0.1 ± 0.1	18.8

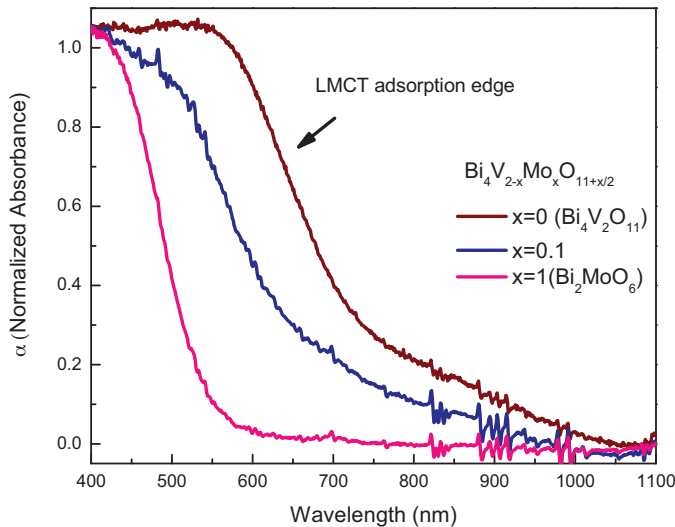


**Fig. 3.** Diffuse reflectance UV–visible absorption spectrum of  $\text{Bi}_4\text{V}_{2-x}\text{Mo}_x\text{O}_{11+x/2}$  measured at 673 K. Labels mark the principal LMCT absorption edge.

The UV–vis diffuse reflectance spectra of  $\text{Bi}_4\text{V}_{2-x}\text{Mo}_x\text{O}_{11+x/2}$  are shown in Fig. 3.  $\text{Bi}_4\text{V}_2\text{O}_{11}$  has the lowest absorption edge, and  $\gamma\text{-Bi}_2\text{MoO}_6$  has the highest absorption edge. The absorption edge for  $\text{Bi}_4\text{V}_{1.9}\text{Mo}_{0.1}\text{O}_{11.05}$  ( $x = 0.1$ ) is lower relative to that for  $\gamma\text{-Bi}_2\text{MoO}_6$ , and exhibits only a single absorption edges. This result indicates that vanadate and molybdate ions are not electronically independent, and there is presumably coupling between Mo and V electronic states. Band gaps were determined from the UV–vis absorption data for the fully oxidized catalyst at 673 K can be calculated using the method described in the Supporting Information, and the results are listed in Table 1.

### 3.2. Measurements of reaction rates and product selectivities

The main products of propene oxidation over  $\text{Bi}_4\text{V}_{2-x}\text{Mo}_x\text{O}_{11+x/2}$  are acrolein,  $\text{CO}_2$ , CO, acetic acid, and acetaldehyde. The rates of propene consumption at 673 K over  $\text{Bi}_4\text{V}_2\text{O}_{11}$ ,  $\text{Bi}_4\text{V}_{1.9}\text{Mo}_{0.1}\text{O}_{11.05}$ , and  $\gamma\text{-Bi}_2\text{MoO}_6$  are presented in Table 2 together with the product selectivities. In all cases, the data have been extrapolated to a propene conversion of zero. The overall activity for propene oxidation increases in the order  $\text{Bi}_4\text{V}_2\text{O}_{11} < \text{Bi}_4\text{V}_{1.9}\text{Mo}_{0.1}\text{O}_{11.05} < \gamma\text{-Bi}_2\text{MoO}_6$ , whereas the selectivity to acrolein increases in the

reverse order and the selectivities to  $\text{CO}_2$  and CO increase in the same order as the overall activity.

The effect of propene conversion on product selectivity was investigated by varying the space velocity of the feed. Fig. 4 shows that while the product selectivity is almost constant with propene conversion for  $\gamma\text{-Bi}_2\text{MoO}_6$ , a very different pattern is observed for  $\text{Bi}_4\text{V}_2\text{O}_{11}$  and  $\text{Bi}_4\text{V}_{1.9}\text{Mo}_{0.1}\text{O}_{11.05}$ . In both cases, the selectivity to acrolein decreases and the selectivities to  $\text{CO}_2$  and CO increase with increasing propene conversion, indicating that acrolein undergoes secondary combustion to  $\text{CO}_x$ . Notably, though, the selectivities to acetaldehyde and acetic acid do not exhibit strong changes with the feed space velocity.

The dependence of the rate of acrolein formation on the partial pressures of propene and oxygen can be expressed in the form of a power-law model given by Eq. (1).

$$\text{rate}_{\text{acrolein}} = k_{\text{app}} P_{\text{C}_3\text{H}_6}^m P_{\text{O}_2}^n \quad (1)$$

where  $k_{\text{app}}$  is the apparent rate coefficient,  $P_i$  is the partial pressure of reactant  $i$ , and  $m$  and  $n$  are the orders in propene and oxygen, respectively. Values for  $m$  and  $n$  at 673 K are given in Table 1 for propene oxidation to acrolein over  $\text{Bi}_4\text{V}_{2-x}\text{Mo}_x\text{O}_{11+x/2}$  ( $x = 0, 0.1$ , and 1.0). The data show that the rate of propene oxidation to acrolein is nearly first-order with respect to the partial pressure of  $\text{C}_3\text{H}_6$  and nearly zero-order with respect to the partial pressures of  $\text{O}_2$ .

Reaction orders for  $\text{C}_3\text{H}_6$  and  $\text{O}_2$  were also measured for the main byproduct produced over  $\gamma\text{-Bi}_2\text{MoO}_6$ ,  $\text{CO}_2$  and CO. The rates of  $\text{CO}_2$  and CO production are both nearly first order in  $\text{C}_3\text{H}_6$ . The partial pressure dependence on  $\text{O}_2$  is 0.4 for  $\text{CO}_2$  and 0.9 for CO, which is consistent with our previous results from  $\alpha\text{-Bi}_2\text{Mo}_3\text{O}_{12}$  [17]. This suggests that the oxygen atoms in  $\text{CO}_2$  come from both gas-phase oxygen and lattice oxygen, and mainly from the gas phase for the production of CO. This is a further indication of the same mechanism for CO and  $\text{CO}_2$  production compared with  $\alpha\text{-Bi}_2\text{Mo}_3\text{O}_{12}$ .

Arrhenius plots for propene oxidation to acrolein over  $\text{Bi}_4\text{V}_{2-x}\text{Mo}_x\text{O}_{11+x/2}$  are shown in Fig. 5 for temperatures in the range of 623–713 K. Values of the apparent activation energy are listed in Table 1. The apparent activation energy for  $\text{Bi}_4\text{V}_{1.9}\text{Mo}_{0.1}\text{O}_{11.05}$  ( $x = 0.1$ ) is similar but higher to that for  $\text{Bi}_4\text{V}_2\text{O}_{11}$ . The apparent activation energy for acrolein production on  $\gamma\text{-Bi}_2\text{MoO}_6$  is 18.8 kcal/mol, but smaller compared than that for  $\alpha\text{-Bi}_2\text{Mo}_3\text{O}_{12}$  19.9 kcal/mol [17]. The values of these activation energies are comparable with those reported by Krenzke et al. [28] for  $\gamma\text{-Bi}_2\text{MoO}_6$  and  $\alpha\text{-Bi}_2\text{Mo}_3\text{O}_{12}$  15 and 18 kcal/mol for temperatures above 693 K.

**Table 2**

Reaction rate of propene consumption and intrinsic selectivity on  $\text{Bi}_4\text{V}_{2-x}\text{Mo}_x\text{O}_{11+x/2}$  for the oxidation of propene at 673 K and  $P_{\text{C}_3\text{H}_6} = P_{\text{O}_2} = 0.167$  atm.

Catalyst	Reaction rate of propene consumption (* $10^{-6}$ mol/min m <sup>2</sup> /cat)	Selectivity (%)				
		Acrolein	CO	$\text{CO}_2$	Acetic Acid	Acetalde-hyde
$\text{Bi}_4\text{V}_2\text{O}_{11}$	1.6	39	15	40	5	1
$\text{Bi}_4\text{V}_{1.9}\text{Mo}_{0.1}\text{O}_{11.05}$	1.9	55	12.5	23	7	2.5
$\text{Bi}_2\text{MoO}_6$	12.4	82	7.5	8	0	2.5

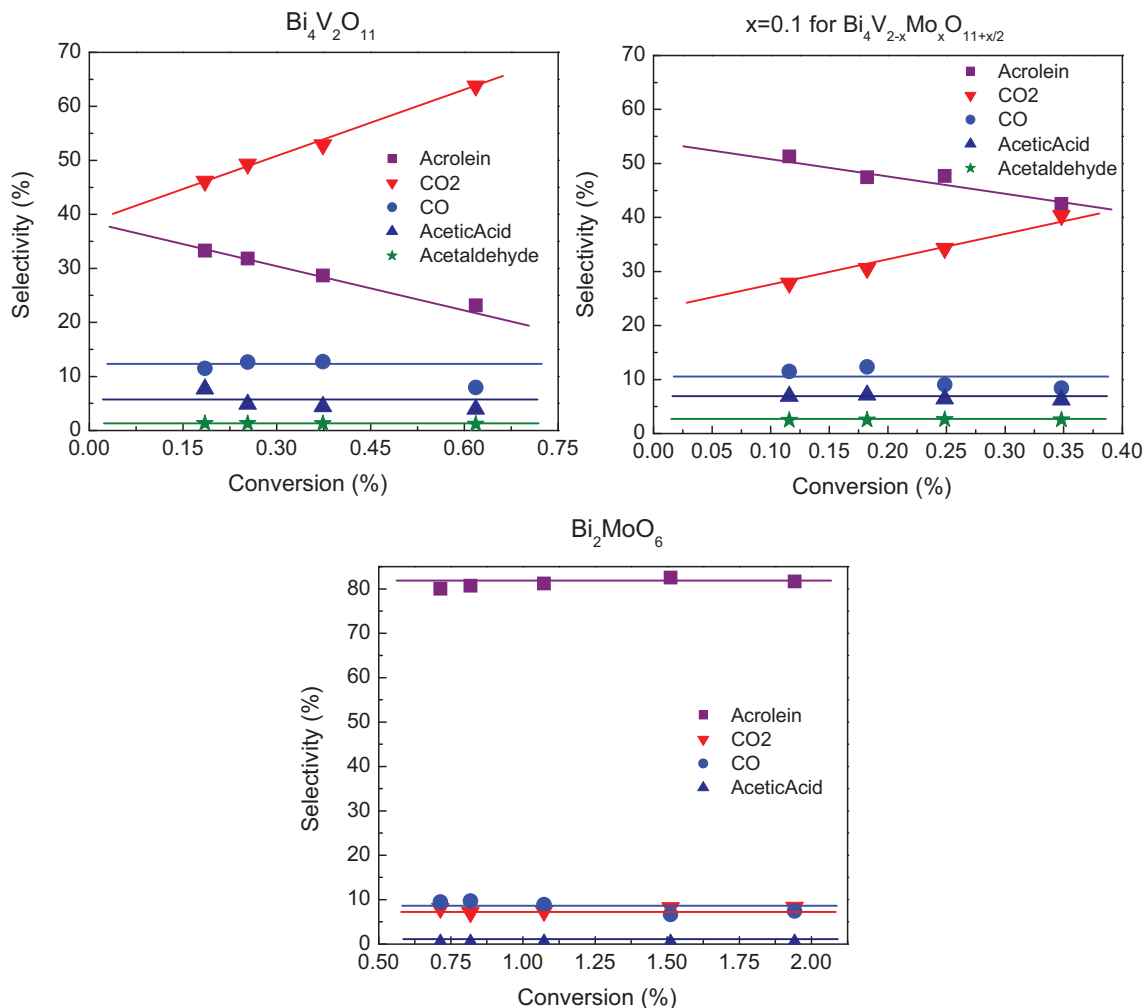


**Fig. 4.** Variation in the selectivity of  $\text{Bi}_4\text{V}_{2-x}\text{Mo}_x\text{O}_{11+x/2}$  for propene oxidation to acrolein at 673 K and  $P_{\text{C}_3\text{H}_6} = P_{\text{O}_2} = 0.167 \text{ atm}$  measured as a function of propene conversion.

#### 4. Discussion

##### 4.1. Mechanism of propene oxidation on $\gamma\text{-Bi}_2\text{MoO}_6$ , $\text{Bi}_4\text{V}_2\text{O}_{11}$ and on $\text{Bi}_4\text{V}_{1.9}\text{Mo}_{0.1}\text{O}_{11.05}$ ( $x=0.1$ )

##### 4.1.1. Mechanism of propene oxidation on $\gamma\text{-Bi}_2\text{MoO}_6$

The kinetics of propene oxidation over  $\gamma\text{-Bi}_2\text{MoO}_6$ , which has an aurivillius structure, and  $\alpha\text{-Bi}_2\text{Mo}_3\text{O}_{12}$ , which has a scheelite structure, are identical. For both catalysts, the rate is first order in the partial pressure of propene and zero order in the partial pressure of oxygen. Isotopic tracer studies for both catalysts show that the reaction proceeds by a Mars van Krevelen mechanism involving oxygen atoms of the lattice [29]. Moreover, the reaction kinetics suggests that the rate-limiting step involves cleavage of a C–H bond in the methyl group of propene [30]. There are also further similarities in the catalytic properties of  $\gamma\text{-Bi}_2\text{MoO}_6$  and  $\alpha\text{-Bi}_2\text{Mo}_3\text{O}_{12}$ . As noted in Table 3, both catalysts exhibit virtually the same activity per unit area and both have very similar activation energies 18.8 kcal/mol for  $\gamma\text{-Bi}_2\text{MoO}_6$  and 19.9 kcal/mol for  $\alpha\text{-Bi}_2\text{Mo}_3\text{O}_{12}$ .

The first question then is whether the type of oxygen atoms involved in the oxidation of propene over  $\alpha\text{-Bi}_2\text{Mo}_3\text{O}_{12}$  and  $\gamma\text{-Bi}_2\text{MoO}_6$  is the same? In situ XANES studies conducted on  $\alpha\text{-Bi}_2\text{Mo}_3\text{O}_{12}$  indicate that Bi remains in the 3+ state and does not undergo reduction, whereas Mo undergoes reduction from the 6+ to the 5+ oxidation state and then is reoxidized in the course of propene oxidation [17]. This conclusion is supported by DFT studies, which reveal further that the most reactive O atoms are those in  $\text{Mo}=\text{O}$

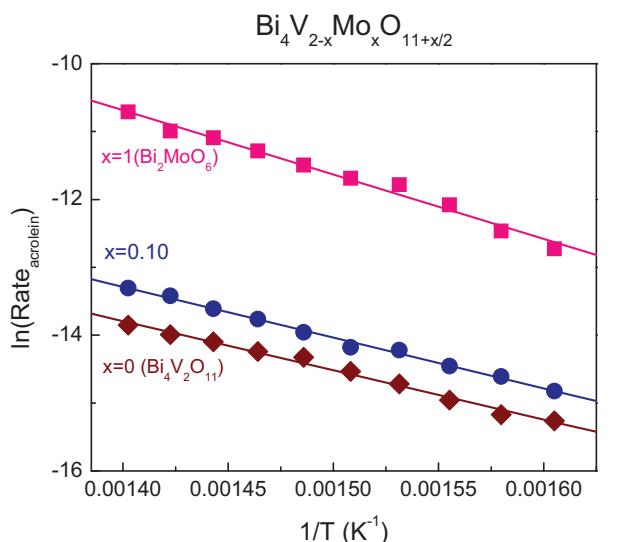


**Fig. 5.** Arrhenius plots for propene oxidation to acrolein over  $\text{Bi}_4\text{V}_{2-x}\text{Mo}_x\text{O}_{11+x/2}$  catalysts. Reaction conditions: T = 623–713 K and  $P_{\text{C}_3\text{H}_6} = P_{\text{O}_2} = 0.167 \text{ atm}$ .

**Table 3**

Apparent rate constant  $k_{app}$  for acrolein production on scheelite catalysts ( $\text{BiVO}_4$  and  $\text{Bi}_2\text{Mo}_3\text{O}_{12}$ ) and aurivilius catalysts ( $\text{Bi}_4\text{V}_2\text{O}_{11}$  and  $\text{Bi}_2\text{MoO}_6$ ).  $P_{\text{C}_3\text{H}_6} = P_{\text{O}_2} = 0.167 \text{ atm}$ , 673 K.

Catalyst	$k_{app}$ ( $\times 10^{-5}$ mol/min $\text{m}^2/\text{cat atm}$ )	Catalyst	$k_{app}$ ( $\times 10^{-5}$ mol/min $\text{m}^2/\text{cat atm}$ )
$\text{BiVO}_4$	17.4	$\text{Bi}_4\text{V}_2\text{O}_{11}$	0.4
$\text{Bi}_2\text{Mo}_3\text{O}_{12}$	6.7	$\text{Bi}_2\text{MoO}_6$	6.4

bonds that interact with the lone pair of proximal Bi atoms (e.g. equatorial Mo=O bonds) [15,16]. This interaction destabilizes the HOMO and stabilizes the LUMO of the molybdate species, thereby facilitating the transfer of an electron into a Mo–O p\* orbital.

By contrast to  $\alpha\text{-Bi}_2\text{Mo}_3\text{O}_{12}$ ,  $\gamma\text{-Bi}_2\text{MoO}_6$  has a layered structure, as shown in Fig. 6. Three different types of oxygens can be distinguished. The first, O<sub>1</sub> is only coordinated to bismuth and is located in the  $(\text{Bi}_2\text{O}_2)^{2+}$  layer. The second type of oxygen, O<sub>2</sub> is located at the top and bottom of the octahedron around the molybdenum and is coordinated to both bismuth and molybdenum. The third type of oxygen, O<sub>3</sub> is in the  $(\text{MoO}_2)^{2-}$  layer and is only coordinated to molybdenum [31].

Several attempts to identify the active form of oxygen in  $\gamma\text{-Bi}_2\text{MoO}_6$  have been reported. Otsubo et al. [32] and Miura et al. [33] prepared  $\gamma\text{-Bi}_2\text{MoO}_6$  by solid-state reaction of  $\text{Bi}_2^{18}\text{O}_3\bullet\text{MoO}_3$  and  $\text{Bi}_2\text{O}_3\bullet\text{Mo}^{18}\text{O}_3$ . While their results suggest that the formation of acrolein formation involves the O<sub>1</sub> atoms of the  $(\text{Bi}_2\text{O}_2)^{2+}$  layers rather than the oxygen atoms of the  $(\text{MoO}_2)^{2-}$  layers, this conclusion is not definitive because at the high temperature required for the synthesis of  $\gamma\text{-Bi}_2\text{MoO}_6$ , oxygen migration occurs readily

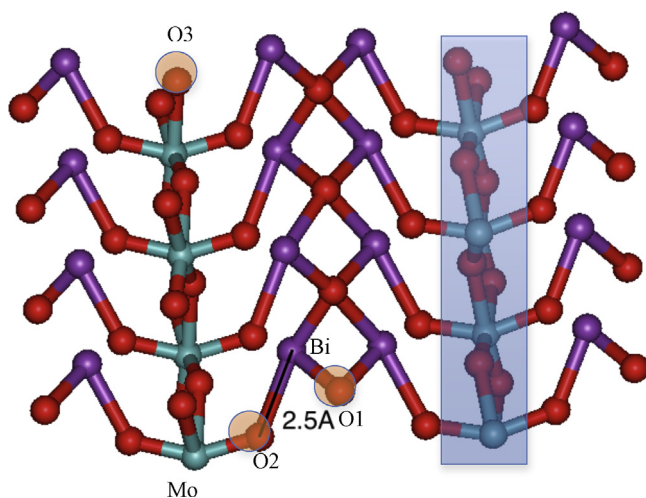
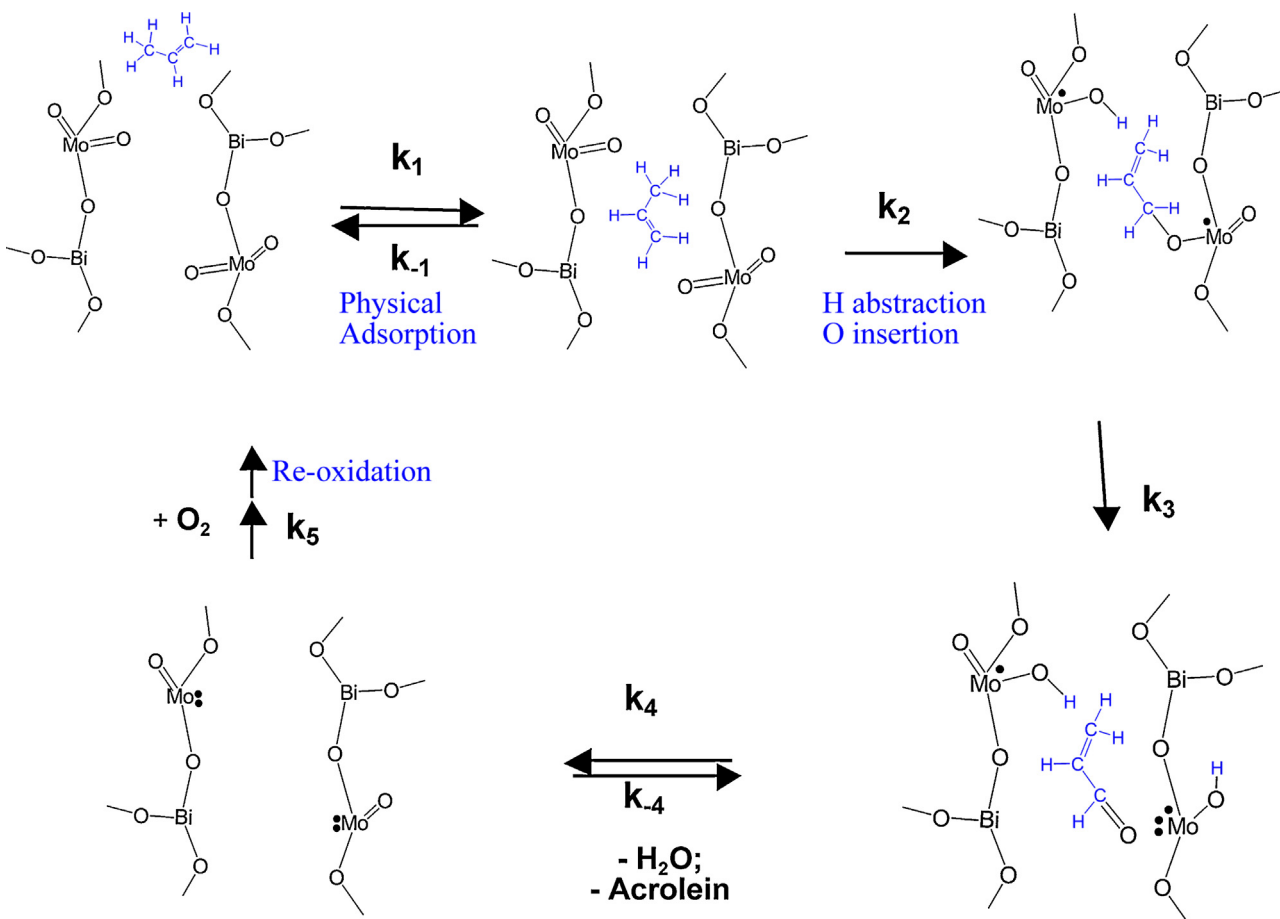


**Fig. 6.**  $\gamma\text{-Bi}_2\text{MoO}_6$  structure. Red: oxygen; Purple: bismuth; Green: molybdenum. O<sub>1</sub>, O<sub>2</sub> and O<sub>3</sub> refer to three different types of oxygen.

leading to complete scrambling of all oxygen atoms [34,35]. The likelihood that O<sub>1</sub> is not the active form of oxygen is supported by the theoretical work of Dadyburjor et al. [36], who calculated the activation energies for the removal of oxygen from  $\gamma\text{-Bi}_2\text{MoO}_6$ . This work revealed that the activation energies for removal of O<sub>1</sub>, O<sub>2</sub>, and O<sub>3</sub> are 80, 2, and 3 eV, respectively. These results suggest that O<sub>2</sub> and O<sub>3</sub> are much more likely to be the active form of O. XPS studies by Ono et al. [37] show that the Mo/Bi ratio at the



**Scheme 1.** The mechanism for the oxidation of propene to acrolein over  $\text{Bi}_2\text{Mo}_3\text{O}_{12}$  proposed on the basis of data reported in this study [17].

surface of  $\gamma\text{-Bi}_2\text{MoO}_6$  is 0.8, suggesting that  $\text{O}_2$  and  $\text{O}_3$  oxygen atoms should be present at the catalyst surface. The strong similarity of the activation energies for propene oxidation over  $\alpha\text{-Bi}_2\text{Mo}_3\text{O}_{12}$  and  $\gamma\text{-Bi}_2\text{MoO}_6$ , also suggests that the oxygen atom involved in the rate-limiting step is similar in both cases. As noted above, in the case of  $\alpha\text{-Bi}_2\text{Mo}_3\text{O}_{12}$  this is the equatorial oxygen, which interacts with the lone pair of Bi in a structure that can be described as  $\text{Bi}\cdots\text{O}=\text{Mo}$ , in which the Bi–O distance is 2.7 Å. Fig. 6 shows that  $\text{O}_2$  is located 2.5 Å from Bi so it is reasonable to expect that  $\text{O}_2$  interacts with Bi in a manner similar to that of the equatorial oxygen atom in  $\alpha\text{-Bi}_2\text{Mo}_3\text{O}_{12}$ . Thus, we propose that the similarities in the activity of  $\gamma\text{-Bi}_2\text{MoO}_6$  and  $\alpha\text{-Bi}_2\text{Mo}_3\text{O}_{12}$  are a consequence of the similarity in the active form of oxygen in both catalysts— $\text{O}_2$  in the case of  $\gamma\text{-Bi}_2\text{MoO}_6$  and equatorial O in the case of  $\alpha\text{-Bi}_2\text{Mo}_3\text{O}_{12}$ .

The kinetics of propene oxidation to acrolein are identical for  $\gamma\text{-Bi}_2\text{MoO}_6$  and  $\alpha\text{-Bi}_2\text{Mo}_3\text{O}_{12}$ . The observed form of the rate expression can be rationalized on the basis of the reaction mechanism shown in Scheme 1 for  $\alpha\text{-Bi}_2\text{Mo}_3\text{O}_{12}$  [17]. As discussed previously, when the catalyst is fully oxidized and propene is weakly adsorbed on the catalyst surface, the rate of propene oxidation to acrolein is given by:

$$\text{rate} = K_1 k_2 P_{\text{C}_3\text{H}_6} [\text{S}] = k_{\text{app}} P_{\text{C}_3\text{H}_6} \quad (2)$$

Here  $k_i$  is the rate coefficient of reaction  $i$ ,  $K_i$  is the equilibrium constant for reaction  $i$ , and  $[\text{S}]$  is the number of activate site per unit BET surface area of the catalyst. In our view, the mechanism shown in Scheme 1 should also apply to propene oxidation over  $\gamma\text{-Bi}_2\text{MoO}_6$ .

#### 4.1.2. Mechanism of propene oxidation on $\text{Bi}_4\text{V}_2\text{O}_{11}$ and on $\text{Bi}_4\text{V}_{1.9}\text{Mo}_{0.1}\text{O}_{11.05}$ ( $x=0.1$ )

While there are similarities in the catalytic properties of  $\text{Bi}_4\text{V}_2\text{O}_{11}$ , which has an aurivillius structure, and  $\text{BiVO}_4$ , which has a scheelite structure, there are also notable differences. The similarity is in the reaction kinetics, for which both catalysts are first order in the partial pressure of propene and zero order in the partial pressure of oxygen. The apparent activation energies are also nearly identical of the two catalysts—14.5 kcal/mol for  $\text{BiVO}_4$  and 14.4 kcal/mol for  $\text{Bi}_4\text{V}_2\text{O}_{11}$ . What is different, though, are the catalyst activity and selectivity. As can be seen in Table 3, the activity of  $\text{BiVO}_4$  for propene oxidation to acrolein is more than 40 times larger than that for  $\text{Bi}_4\text{V}_2\text{O}_{11}$  under identical reaction conditions. Table 2 also shows that the intrinsic selectivity to acrolein is significantly higher for  $\text{BiVO}_4$  (76%) than that for  $\text{Bi}_4\text{V}_2\text{O}_{11}$  (39%). It is notable, though, that both catalysts show a monotonic decrease in the acrolein selectivity and corresponding rise in the selectivity to  $\text{CO}_2$  with increasing propene conversion, whereas the selectivities to  $\text{CO}$ ,  $\text{CH}_3\text{COOH}$ , and  $\text{CH}_3\text{CHO}$  remain constant with propene conversion. These trends indicate that acrolein readily undergoes combustion to  $\text{CO}_2$  over both  $\text{BiVO}_4$  and  $\text{Bi}_4\text{V}_2\text{O}_{11}$  as the concentration of acrolein in contact with the catalyst increases. The differences in the activity and selectivity of  $\text{Bi}_4\text{V}_2\text{O}_{11}$  and  $\text{BiVO}_4$  are attributed to differences in the activity of the oxygen atoms present at the surface of the two materials. As discussed below, the O atoms present at the surface of  $\text{Bi}_4\text{V}_2\text{O}_{11}$  are significantly more active than those at the surface of  $\text{BiVO}_4$ . This difference can lead to higher rates of oxidation of the vinylalkoxide intermediate to acrolein (Scheme 1) and consequently to a lower intrinsic selectivity to acrolein, as well as to a greater tendency for acrolein to combust as the acrolein concentration increases with increasing propene conversion. The points are discussed in more detail below.

For molybdenum-substituted  $\text{Bi}_4\text{V}_2\text{O}_{11}$ ,  $\text{Bi}_4\text{V}_{1.9}\text{Mo}_{0.1}\text{O}_{11.05}$  ( $x=0.1$ ), the activity and intrinsic selectivity of acrolein formation are higher than that of  $\text{Bi}_4\text{V}_2\text{O}_{11}$  (Table 2) but still lower than that of  $\text{BiVO}_4$ . Fig. 4 also shows that with increasing propene

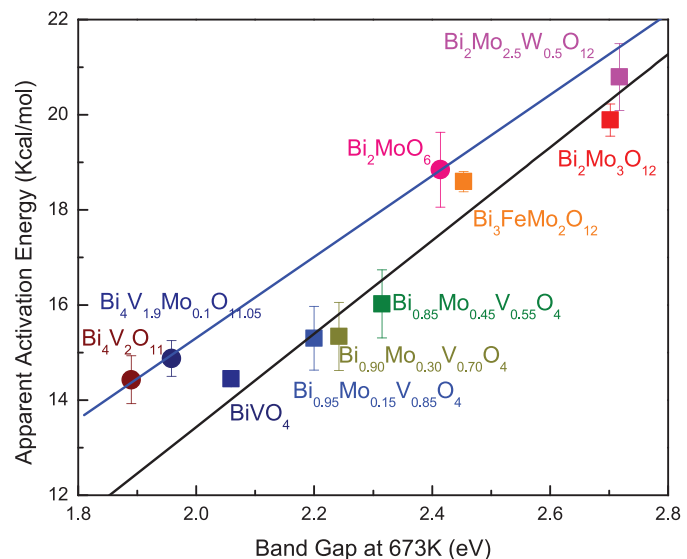


Fig. 7. Apparent activation energies for oxidation of propene to acrolein versus the band gap measured at 673 K for catalysts having the scheelite (lower line, square) and aurivillius (upper line, circle) structures. Reaction conditions: T=673 K and  $P_{\text{C}_3\text{H}_6} = P_{\text{O}_2} = 0.167$  atm.

conversion, the selectivity to acrolein decreases and that to  $\text{CO}_2$  increases. Further discussion of these trends is given below.

#### 4.2. Band-gap energy as a descriptor of activation energy

We have recently shown that the apparent activation energy for propene oxidation to acrolein correlates with the band gap of catalyst of varying composition but all having a scheelite structure. This relationship has been rationalized on the basis of a Born-Haber cycle and the recognition that the largest contributor to this cycle is the band-gap energy, which is also the component most dependent on catalyst composition [21]. The question that we now ask is whether a similar correlation holds for catalysts having the aurivillius structure.

Fig. 7 shows that the apparent activation energy for propene oxidation correlates linearly with the band gap for catalyst of different

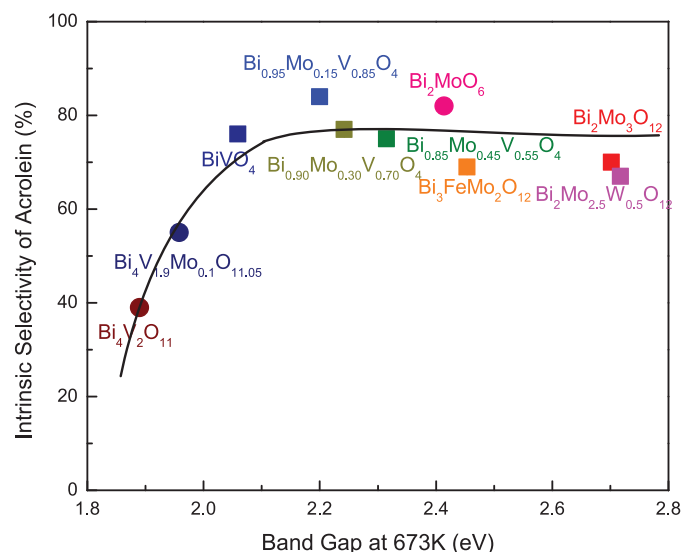
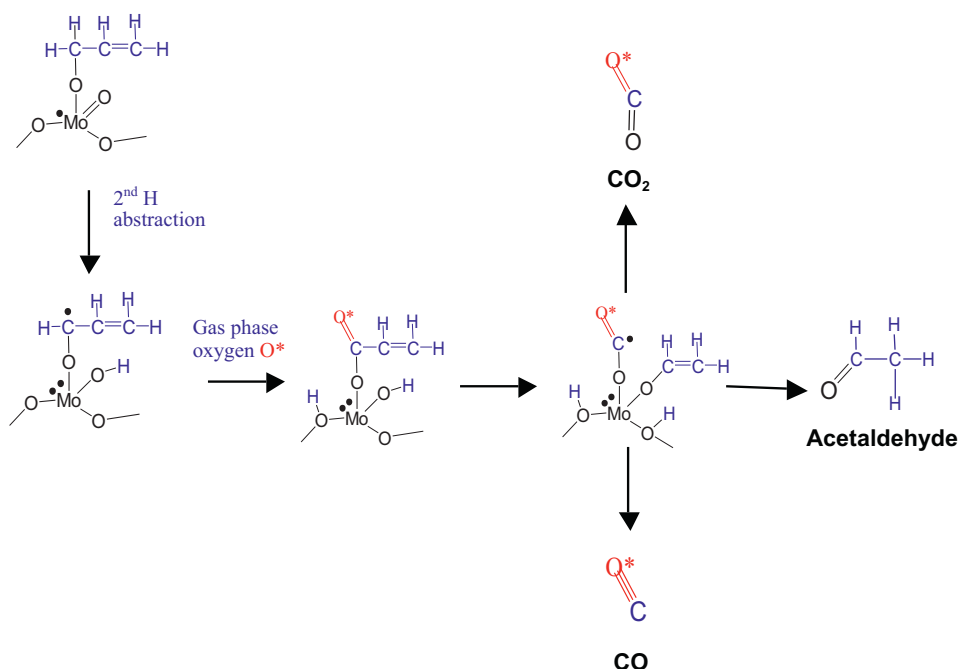


Fig. 8. Intrinsic selectivity to acrolein versus the band gap measured at 673 K (scheelite, square; aurivillius, circle). Reaction conditions: T=673 K and  $P_{\text{C}_3\text{H}_6} = P_{\text{O}_2} = 0.167$  atm.



**Scheme 2.** Possible pathway for CO and  $CO_2$  formation on  $Bi_2MoO_6$  during the oxidation of propene [17].

composition having either the scheelite or aurivillius structure. The only difference is that for the same band gap, the apparent activation energies are about 1.5 kcal/mol higher for catalysts with the aurivillius than the scheelite structure. Since the apparent activation energy is the sum of the enthalpy of propene adsorption and the intrinsic activation energy, we propose that the slightly higher activation energies observed for catalysts with the aurivillius structure compared with the scheelite structure is due the slightly lower heat of adsorption for propene on the former structure. Unfortunately, to the best of our knowledge, the difference in the heat of adsorption for the two types of structures has not been reported, and, therefore, we cannot verify this hypothesis.

The results presented in Fig. 7 suggest that catalysts with low band gaps should be exhibit a higher activity for propene oxidation to acrolein per active site than those with higher band gaps. While this conclusion is true for catalysts with band gaps above about  $\sim 2.1$  eV, it does not hold for catalyst with lower band gaps. As shown in this study for  $Bi_4V_2O_{11}$  and  $Bi_4V_{1.9}Mo_{0.1}O_{11.05}$ , and reported earlier for  $BiVO_4$ , catalysts with band gaps below  $\sim 2.1$  eV show both lower intrinsic selectivities to acrolein and higher activity for acrolein combustion. This pattern is nicely illustrated in Fig. 8. Two factors can account for the loss of acrolein selectivity for catalysts with band gaps  $< 2.1$  eV. Scheme 2 shows a possible pathway for the oxidation of the vinylalkoxide formed as an intermediate leading to acrolein [17]. Loss of an H atom from this intermediate initiates a cascade of steps leading to CO and  $CO_2$ . It is notable that the participation of an oxygen atom from  $O_2$  adsorbed from the gas phase accounts for the observed positive order in oxygen partial pressure of the rate of  $CO_x$  formation. Clearly then, the more active the surface oxygen, the higher will be the rate of  $CO_x$  formation paralleling the rate of acrolein formation. A high chemical activity of surface oxygen could also be responsible for the secondary combustion of acrolein.

## 5. Conclusions

The oxidation of propene to acrolein has been investigated over aurivillius-structured mixed metal oxides,  $\gamma$ - $Bi_2MoO_6$ ,  $Bi_4V_2O_{11}$ ,

and Mo-substituted  $Bi_4V_2O_{11}$ , and the activity and selectivity of these materials are compared with those for similar catalysts prepared with the scheelite structure. All of the catalysts exhibit similar kinetics—the rate of acrolein formation is first order in the partial pressure of propene and zero order in the partial pressure of oxygen. These kinetics can be rationalized on the basis of the mechanism shown in Scheme 1. Both sets of catalysts show a linear correlation in the apparent activation energy with the band gap of the catalyst measured at the reaction conditions (Fig. 7). However, for the same band gap, the apparent activation energy for propene oxidation to acrolein is about 1.5 kcal/mol higher for catalysts having the aurivillius structure. This difference is attributed to the lower heat of propene adsorption on the aurivillius structure. The results of this study also reveal another interesting feature. As seen in Fig. 8, catalysts with band gaps of above  $\sim 2.1$  eV exhibit high intrinsic acrolein selectivities,  $\sim 75\%$ , whereas catalysts with band gaps below  $\sim 2.1$  eV exhibit significant lower intrinsic acrolein selectivities. It is also observed that the acrolein selectivity is independent of propene conversion for catalysts with band gaps above  $\sim 2.1$  eV, whereas catalysts with band gaps below  $\sim 2.1$  eV exhibit a strong decrease in acrolein selectivity with increasing propene conversion as a consequence of acrolein combustion. These findings clearly indicate that there is no advantage to developing propene oxidation catalysts with band gaps below  $\sim 2.1$  eV.

## Acknowledgments

This work was funded by the U.S. Department of Energy, Office of Basic Science, Chemical Science Division, under Contract No. DE-AC02-05CH11231.

## Appendix A. Supplementary data

Supplementary data associated with this article can be found, in the online version, at <http://dx.doi.org/10.1016/j.cattod.2015.06.011>

## References

- [1] G.W. Keulks, L.D. Krenzke, T.M. Notermann, *Adv. Catal.* 27 (1978) 183–225.
- [2] G. Ertl, H. Knozinger, F. Schuth, J. Weitkamp (Eds.), *Handbook of Heterogeneous Catalysis*, Wiley-VCH, Weinheim, Germany, 2008, p. 3481.
- [3] Y. Moro-Oka, W. Ueda, *Adv. Catal.* 40 (1994) 233–273.
- [4] J.M.M. Millet, H. Ponceblanc, G. Coudurier, J.M. Herrmann, J.C. Vedrine, *J. Catal.* 142 (1993) 381–391.
- [5] D. Carson, G. Coudurier, M. Forissier, J.C. Vedrine, *J. Chem. Soc. Faraday Trans. I* 79 (1983) 1921–1929.
- [6] H.H. Voge, C.D. Wagner, D.P. Setvenson, *J. Catal.* 2 (1963) 58–62.
- [7] W.M.H. Sachtler, *Rec. Trav. Chim.* 82 (1963) 243–245.
- [8] B. Grzybowska, J. Haber, J. Janas, *J. Catal.* 49 (1977) 150–163.
- [9] W. Ueda, K. Asakawa, C.L. Chen, Y. Moro-Oka, T. Ikawa, *J. Catal.* 101 (1986) 360–368.
- [10] G.W. Keulks, *J. Catal.* 19 (1970) 232–235.
- [11] J. Haber, W. Turek, *J. Catal.* 190 (2000) 320–326.
- [12] R.K. Grasselli, *Top. Catal.* 21 (2001) 79–88.
- [13] R.K. Grasselli, *J. Chem. Educ.* 63 (1986) 216–221.
- [14] L.C. Glaeser, J.F. Brazdil, M.A. Hazle, M. Mehicic, R.K. Grasselli, *J. Chem Soc., Faraday Trans. I* 81 (1985) 2903–2912.
- [15] A. Getsoian, V. Shapovalov, A.T. Bell, *J. Phys. Chem. C* 117 (2013) 7123–7137.
- [16] A. Getsoian, A.T. Bell, *J. Phys. Chem. C* 117 (2013) 25562–25578.
- [17] Z. Zhai, A. Getsoian, A.T. Bell, *J. Catal.* 308 (2013) 25–36.
- [18] P. Porta, M.L. Jacono, M. Valigi, G. Minelli, A. Anichini, S.D. Rossi, D. Gazzoli, *J. Catal.* 100 (1986) 86–94.
- [19] S.D. Rossi, M.L. Jacono, P. Porta, M. Valigi, D. Gazzoli, G. Minelli, A. Anichini, *J. Catal.* 100 (1986) 95–102.
- [20] D. Cordischi, M.L. Jacono, D. Gazzoli, G.P. Minelli, *Porta. J. Catal.* 102 (1986) 1–9.
- [21] A. Getsoian, Z. Zhai, A.T. Bell, *J. Am. Chem. Soc.* 136 (2014) 13684–13697.
- [22] K.R. Kendall, C. Navas, J.K. Thomas, H. Loyer, Recent developments in oxide ion conductors: aurivillius phases 15 (1996) 642–649.
- [23] B. Senthilkumar, R. Kalai Selvan, L. Vasylechko, M. Minakshi, *Solid State Sci.* 35 (2014) 18–27.
- [24] G. Mairesse, P. Roussel, R.N. Vannier, M. Anne, G. Nowogrocki, *Solid State Sci.* 5 (2003) 861–869.
- [25] A. Phuruangrat, P. Jitrou, P. Dumrongrojathanath, N. Ekthammathat, B. Kuntalue, S. Thongtem, T. Thongtem, *J. Nanomater.* 2013 (2013) 1–8.
- [26] A.M. Cruz, S.O. Alfaro, *J. Mol. Catal. A Chem.* 320 (2010) 85–91.
- [27] S.J. Patwe, A. Patra, R. Dey, A. Roy, R.M. Kadam, S.N. Achary, A.K. Tyagi, *J. Am. Ceram. Soc.* 96 (2013) 3448–3456.
- [28] L.D. Krenzke, G.W. Keulks, *J. Catal.* 64 (1980) 295–302.
- [29] L.D. Krenzke, G.W. Keulks, *J. Catal.* 61 (1980) 316–325.
- [30] C.R. Adams, T.J. Jennings, *J. Catal.* 3 (1964) 549–558.
- [31] R.G. Teller, J.F. Brazdil, R.K. Grasselli, *Acta Cryst. C40* (1984) 2001–2005.
- [32] T.-T. Otsubo, H. Miura, Y. Morikawa, T. Shirasaki, *J. Catal.* 36 (1975) 240–243.
- [33] H. Miura, T.-T. Otsubo, T. Shirasaki, Y. Morikawa, *J. Catal.* 56 (1979) 84–87.
- [34] E.V. Hoefs, J.R. Monnier, G.W. Keulks, *J. Catal.* 57 (1979) 331–337.
- [35] L.T. Sim, C.K. Lee, A.R. West, *J. Mater. Chem.* 12 (2002) 17–19.
- [36] D.B. Dadyburjor, E. Ruckenstein, *J. Catal.* 63 (1980) 383–388.
- [37] T. Ono, K. Utsumi, S. Tsukamoto, H. Tamaru, M. Kataoka, F. Noguchi, *J. Mol. Catal. A Chem.* 318 (2010) 94–100.